Supporting Information

New Insights into Traditional Charge Compensation Theory: Amphoteric Behavior of TiO_2 under the Guidance of Supply-Demand Relationship

Zhisheng Bi [a], Kejiang Li [*, a], Chunhe Jiang [a], Jianliang Zhang [a], Shufang Ma [a], Conejo Alberto [a], Minmin Sun [a], Yushan Bu [a], Mansoor Barati [b], Shan Ren [*, c]

[a] School of Metallurgical and Ecological Engineering, University of Science and Technology Beijing, Beijing 100083, P.R. China

[b] Department of Materials Science and Engineering, University of Toronto, Toronto, ON M5S 3E4, Canada

[c] School of Materials Science and Engineering, Chongqing University, Chongqing 400044, P.R. China

*Corresponding author: Kejiang Li, Shan Ren

Address:

Kejiang Li: 30 Xueyuan Rd., Haidian District, Beijing 100083, PR China.

Shan Ren: No.174 Shazheng Rd., Shapingba District, Chongqing 400044, P.R. China

E-mail: likejiang@ustb.edu.cn (Kejiang Li); shan.ren@cqu.edu.cn (Shan Ren)

1. Computational Methodology

1.1. Simulation methods

In the present molecular dynamics simulation, nearly 10000 atoms were selected to be put into a cubic box. The components of studied systems have been listed in Table. S1. The variables studied are TiO_2 contents and basicity and the temperature was kept at 2273 K (absolute temperature). The notation of B*i*T*j* indicates that the different TiO_2 contents and basicity. In which B represents the basicity, T represents the TiO_2, *i* equals 1, 2, 3, 4 respectively (representing the corresponding basicity of 0.5, 0.9, 1.3 and 1.7 respectively), and *j* equals 1, 2, 3, 4, 5, 6 respectively (representing the TiO_2 contents of 10 wt.%, 15 wt.%, 20 wt.% , 25 wt.% , 30 wt.% and 35 wt.% respectively). Newton's law of motion, NVT (Number of particles, System Volume, Temperature) ensemble and periodic boundary conditions were applied to this simulation.

Table. S1 Components of the studied blast furnace slag system

Basicity	Samples	Si atoms	Ca atoms	Ti atoms	O atoms	Sum
B=0.5	B1T1	2248	1205	282	6265	10000
	B1T2	2142	1147	427	6285	10001
	B1T3	2033	1089	574	6303	9999
	B1T4	1923	1030	723	6322	9998
	B1T5	1811	970	876	6344	10001
	B1T6	1697	909	1031	6365	10002
B=0.9	B2T1	1850	1784	294	6072	10000
	B2T2	1759	1696	444	6102	10001
	B2T3	1666	1607	596	6131	10000
	B2T4	1573	1517	749	6161	10000
	B2T5	1478	1425	905	6191	9999
	B2T6	1382	1332	1063	6222	9999
B=1.3	B3T1	1572	2189	302	5937	10000
	B3T2	1492	2078	456	5974	10000
	B3T3	1412	1966	611	6012	10001
	B3T4	1330	1853	768	6049	10000
	B3T5	1248	1739	926	6087	10000
	B3T6	1165	1623	1086	6125	9999

B=1.7	B4T1	1366	2488	308	5836	9998
	B4T2	1296	2360	464	5880	10002
	B4T3	1225	2230	622	5924	10001
	B4T4	1153	2100	781	5968	9998
	B4T5	1081	1968	941	6012	10001
	B4T6	1008	1835	1102	6055	10002

Table. S2. BMH model parameters used in this simulation [1, 2].

i	j	A_{ij} (gÅ²/fs²)	B_{ij} (1/Å)	C_{ij} (gÅ^8/fs²)	D_{ij} (gÅ^{10}/fs²)
Si	Si	3.47E-23	6.25	0.00	0.00
Si	Ca	4.28E-22	6.25	0.00	0.00
Si	Ti	1.40E-22	6.25	0.00	0.00
Si	O	1.01E-21	6.06	0.00	0.00
Ca	Ca	5.27E-21	6.25	6.95E-26	0.00
Ca	Ti	1.72E-21	6.25	0.00	0.00
Ca	O	1.15E-20	6.06	1.39E-25	0.00
Ti	Ti	5.63E-22	6.25	0.00	0.00
Ti	O	3.89E-21	6.06	0.00	0.00
O	O	2.40E-20	5.88	2.78E-25	0.00

After obtaining the data, the radial distribution functions (RDFs), oxygen network structure, polymerization degree of system, viscosity ware analyzed by using tools such as VMD [3] and ISSACS [4]. All the computations were performed on the GPC supercomputer at the SciNet HPC Consortium in the Compute/Calcul Canada national computing platform [5, 6].

1.2. Calculation methods

Coordination numbers (CNs) represent the number of the first neighbor atoms (O atoms) of an atom (B atom), which are obtained by integrating the first peak and valley of the CNs and the formula (equation. 1) is as follows:

$$N_{ij}(r) = \frac{4\pi N_j}{V}\int_0^r r^2 g_{ij}(r)dr \quad (1)$$

Radial distribution functions (RDFs) describe the distribution of other ions around an ion, and characterize the probability of finding other ions around an ion. Therefore, the RDFs are the best parameters to explain whether the potential function and its parameters match the system. The equation. 2 lists the mathematical expression of RDFs.

$$g_{ij}(r) = \frac{v}{N_i N_j} \sum_j \frac{n(r)}{4\pi r^2 \Delta r} \tag{2}$$

2. Results and discussion

2.1. Radial Distribution Functions (RDFs) and Bond Length

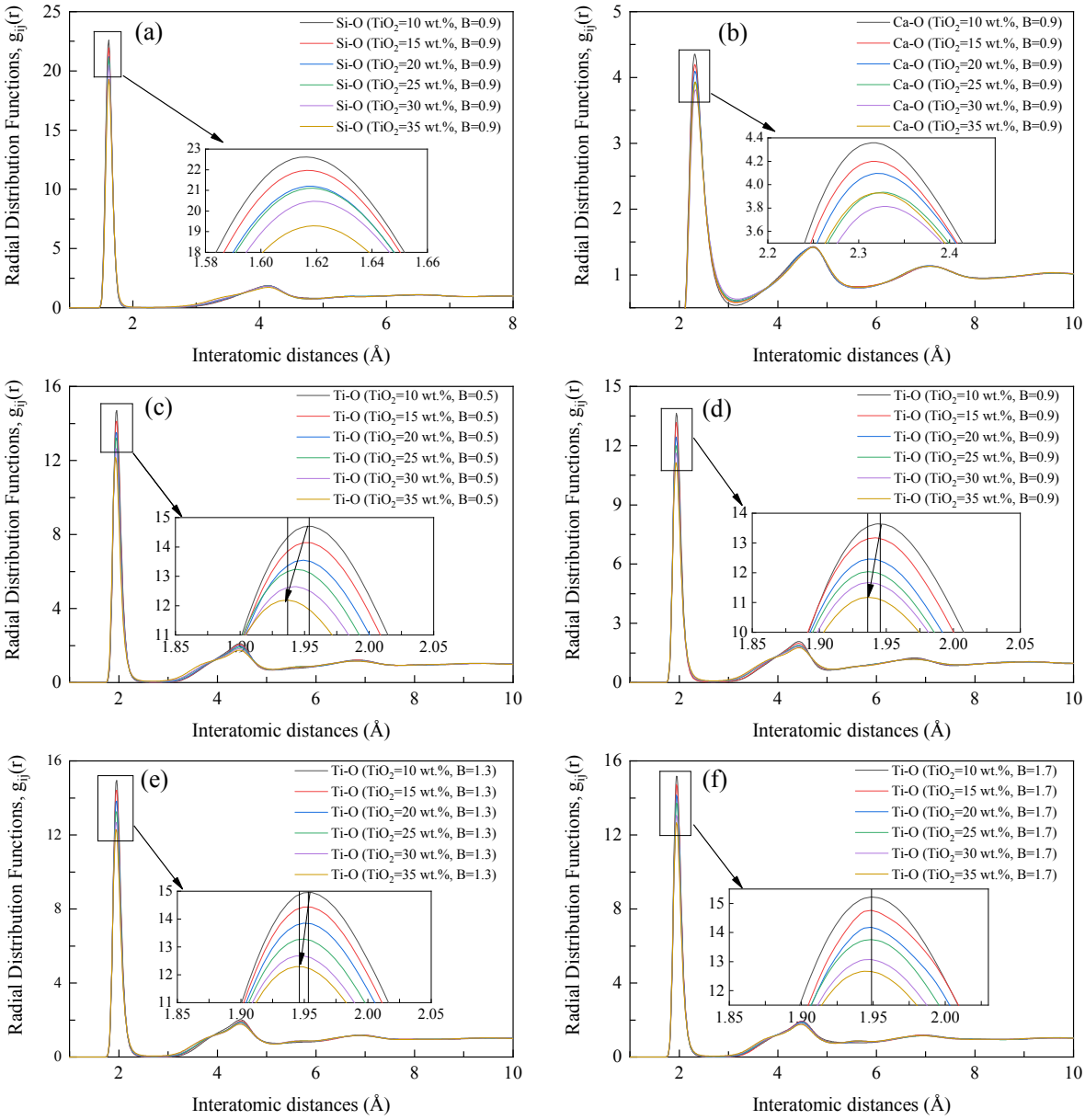

Figure S1. RDFs under different TiO_2 contents and basicity conditions. The first peak of each figure is enlarged and the vertical lines perpendicular to the abscissa axis in the enlarged view highlight the peak value under the corresponding radial distribution functions: (a) the RDFs of Si-O atoms (influence of TiO_2); (b) the RDFs of Ca-O atoms (influence of TiO_2); (c-f) the RDFs of Al-O atoms (influence of TiO_2 and basicity).

To facilitate analysis, the RDFs between various cations and oxygen ions of representative samples were plotted and shown in Figure S1. The first peak of each graph in Figure S1 is the most probable bond distances of the corresponding ion-pair, which is used to estimate the corresponding bond length. The r_1 is the abscissa of the first peak of the radial distribution function of the corresponding ion-pair, representing the nearest neighbor bond length of the ion-pair. Previous experiments and simulations [7-10] have proved that the r_1 of Si-O bonds should be between 1.61-1.62Å, the r_1 of Ca-O bonds should be between 2.29-2.83Å, the r_1 of Ti-O bonds should be between 1.82-2.18Å.

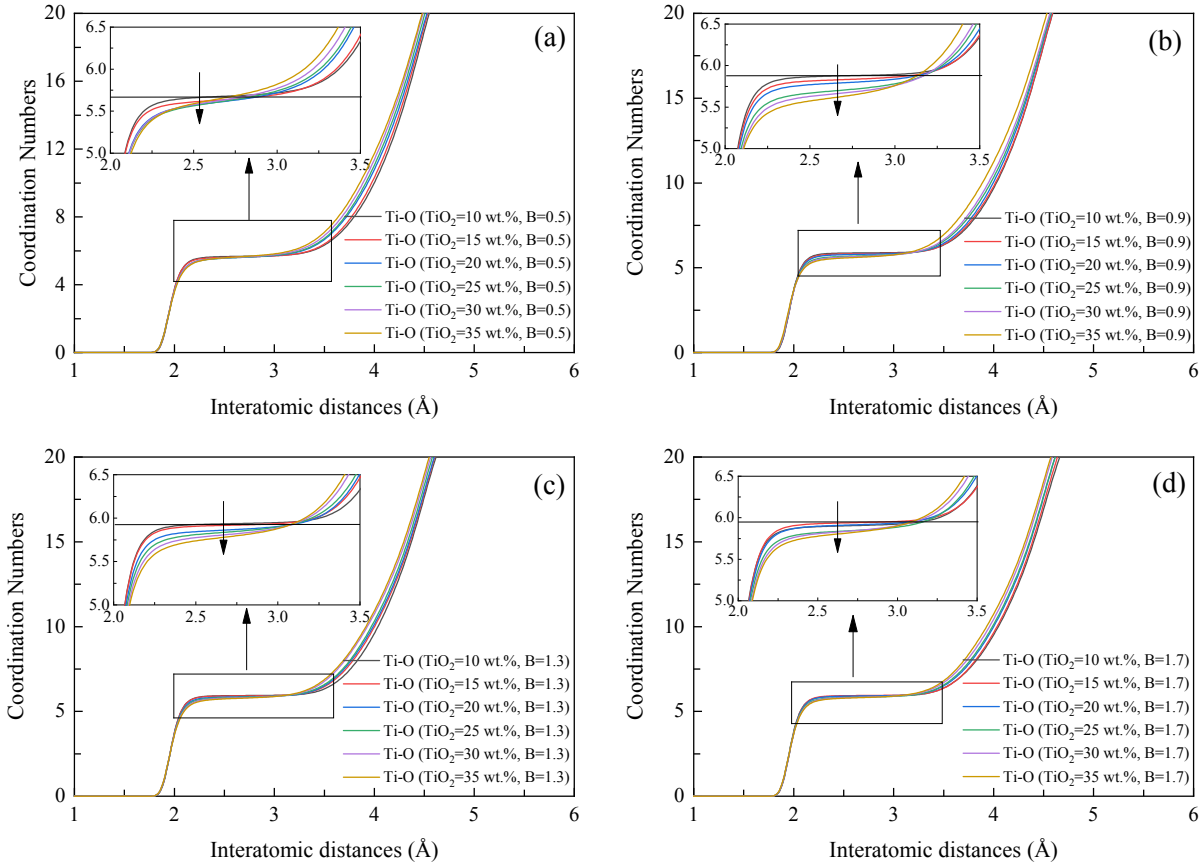

Figure S2. CNs of O atoms around Ti atoms under different TiO_2 contents and basicity conditions. The part where the slope of the coordination number curve is close to zero is enlarged and put into each figure and the straight lines parallel to the abscissas in the partial enlarged view mark the maximum coordination number in the samples: (a) variation of CNs with TiO_2 contents when basicity is 0.5; (b) variation of CNs with TiO_2 contents when basicity is 0.9; (c) variation of CNs with TiO_2 contents when basicity is 1.3; (d) variation of CNs with TiO_2 contents when basicity is 1.7.

2.2. Bond Angle and Local Structure Evolution

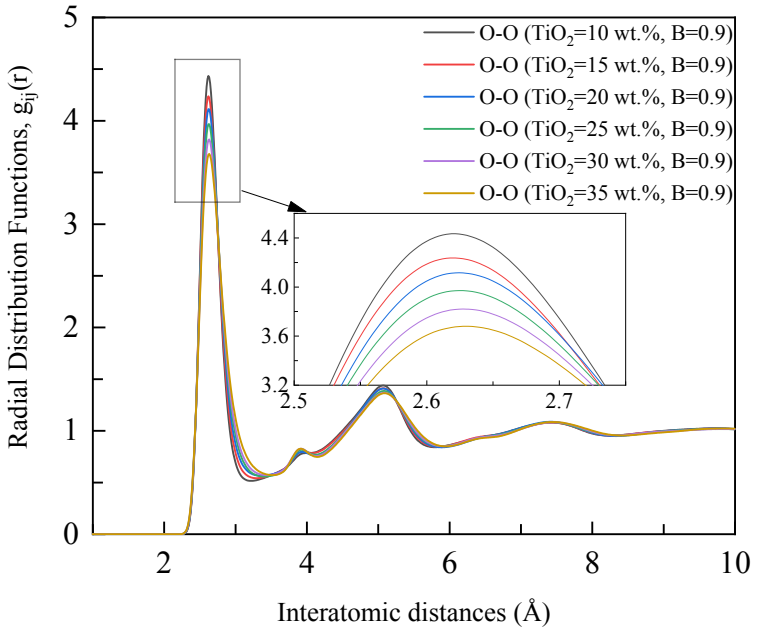

Figure S3. O-O RDFs under different TiO_2 contents and basicity conditions.

.

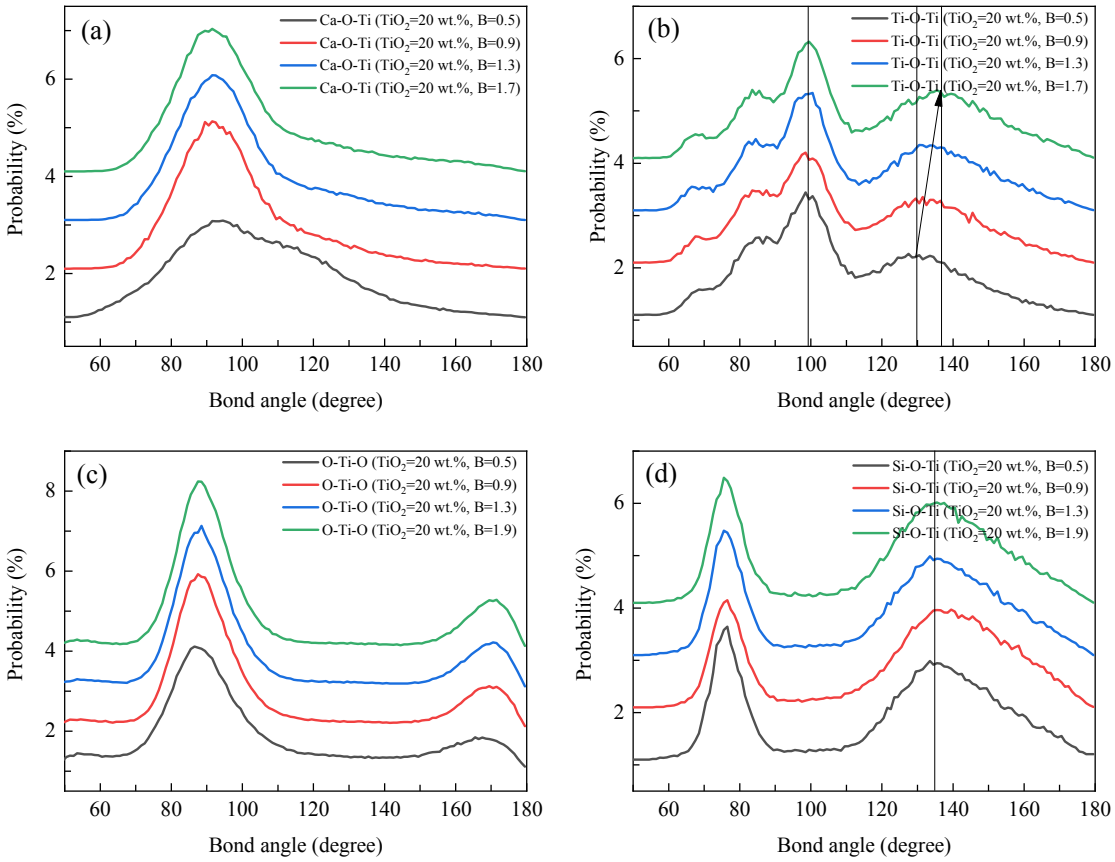

Figure S4. Change situation of bond angle with the basicity. Part peak values are marked with straight lines perpendicular to the abscissa axis, and the arrows on the way point to the change situation of peak value with the basicity: (a) variation of Ca-O-Ti bond angle with the basicity; (b) variation of Ti-O-Ti bond angles with the basicity; (c) variation of O-Ti-O bond angles with the basicity; (d) variation of Si-O-Ti bond angles with the basicity.

2.3. Oxygen Network Structure and Global Structural Stability

For the microstructure of the system, it is very important to study the contents of bridge oxygen (BO) and non-bridge oxygen (NBO). Besides BO and NBO, the network structure of oxygen also includes free oxygen (FO) and oxygen triclusters (TO). Schematic diagrams of the percentage content of different types of oxygen are shown in Figure S5.

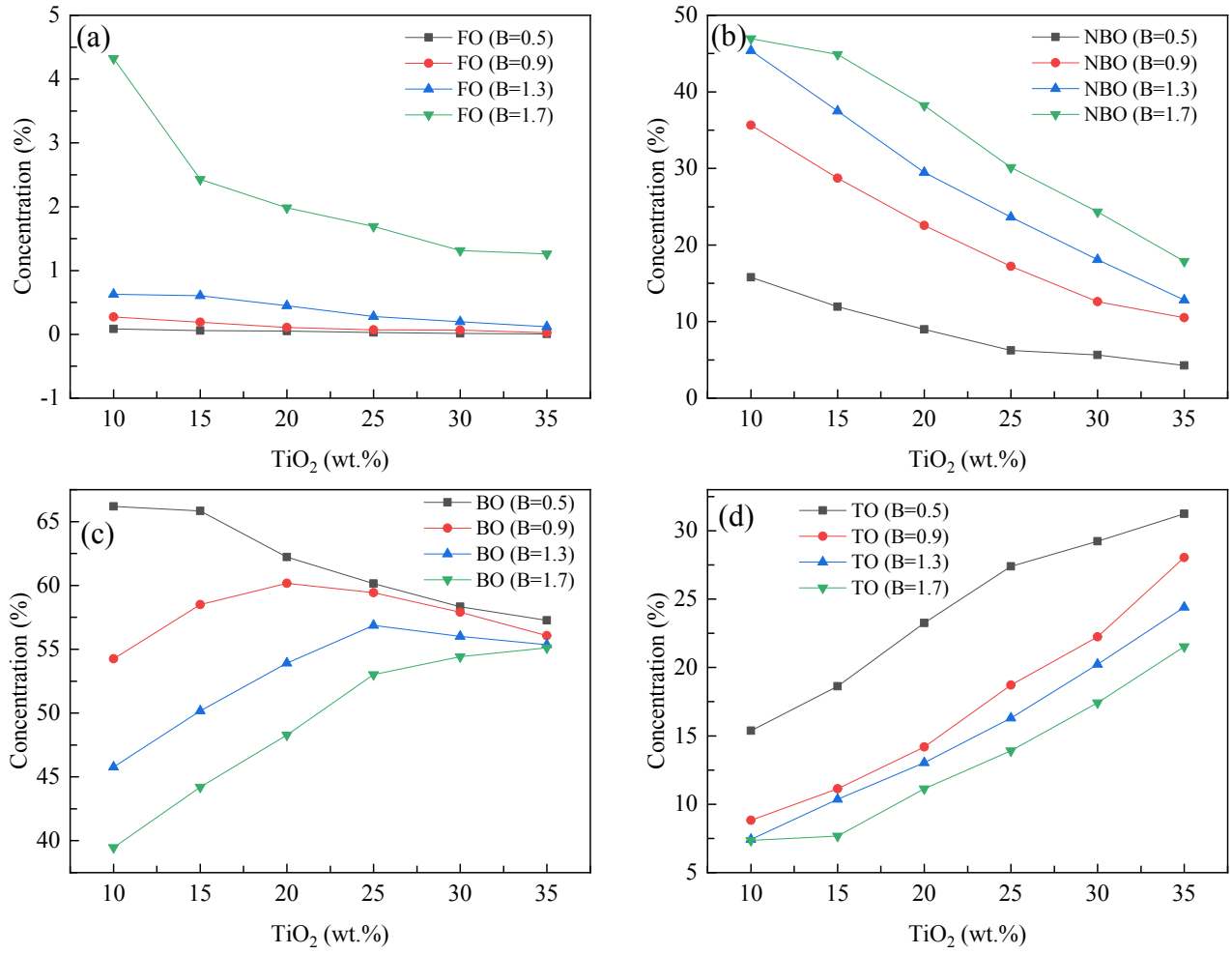

Figure S5. The concentrations of various types of oxygen with different TiO_2 contents and basicity. Among them, the influence of TiO2 contents on different types of oxygen atoms is studied horizontally, and the influence of basicity on different types of oxygen atoms is compared vertically: (a) effect of basicity and TiO_2 contents on FO contents; (b) effect of basicity and TiO_2 contents on NBO contents;

(c) effect of basicity and TiO_2 contents on BO contents; (d) effect of basicity and TiO_2 contents on TO contents.

From the point of view of global structure, with the increase of TiO_2 contents in the system, free oxygen and non-bridge oxygen in the system have been decreasing (Figure S5(a-b)), which is because Ti^{4+} ions tend to form TiO_6 octahedrons with O^{2-} ions, and the charge of non-bridge oxygen ions is not saturated, there is an active site left. Therefore, Ti^{4+} ions have strong binding ability with free oxygen and non-bridge oxygen in the system, which leads to the decrease of free oxygen and non-bridge oxygen contents in the system. Longitudinal analyses of Figure S5(a-b) show that the contents of free oxygen and non-bridge oxygen in the system with higher basicity are higher than that in the system with lower basicity. High basicity provides more Ca^{2+} ions and O^{2-} ions for the system, which alleviates the situation that free oxygen and non-bridge oxygen can't satisfy Ti^{4+} ions, which makes the system with high basicity have higher free oxygen and unbridged oxygen contents.

Bridge oxygen, as the connecting bridge of polyhedral structures under the microscopic view of the system, is very important to study the global atomic structure. The existing publications [11-13] have explained that TiO_2 is an amphoteric oxide, and this simulation also proves that TiO_2 does have amphoteric transformation behavior from the perspective of atomic structure, and the show acid-base properties behavior is affected by the basicity of the system. In the text, the changes and reasons of the bond angle in Figure S5c are analyzed in detail. The variation of the content of system TO is shown in Figure S5d. It could be found that the contents of TO always increase with the increase of TiO_2 contents under any basicity conditions. Combined with Figure 5c, it could be proved that when excessive Ti^{4+} ions compete with other polyhedral structures for oxygen atoms, this part of the contended oxygen

atoms is changed from BO to TO. Therefore, the BO contents of the system decrease and the TO contents increase.

In addition, through the basic equivalent idea, the calculation model of oxide amphoteric transformation can be established. There are three basic facts or assumptions in this model. First: oxygen ion is the only negative charge carrier of the system, and the balance between supply and demand of oxygen ion is the basic relationship of supply and demand theory Second: all polyhedral structures of the system are connected by oxygen ions. Third: NBO is equivalent to 0.5 BO, and TO oxygen is equivalent to 1.5 BO. The model calculation formula is as follows:

$$\Delta N(O) = N(O)_{supplied} - N(O)_{demanded} \quad (3)$$

$$N(O)_{supplied} = 2 \times \mathrm{R} \times N_O \quad (4)$$

$$\mathrm{R} = \frac{\sum(0.5 \times P_{NBO} + P_{BO} + 1.5 \times P_{TO})}{N_{sample}} \quad (5)$$

$$N(O)_{demanded} = \sum(N_i \times P_i \times i) \quad (6)$$

The core of the supply-demand relationship model is to virtualized break the complex network structure of the system. Through $N(O)_{demanded}$, the number of equivalent oxygen atoms demanded by the polyhedron in the system can be clarified. Then use $N(O)_{supplied}$ to calculate the number of equivalent oxygen atoms that the system can supply. The difference is the balance between supply and demand. In which $\Delta N(O)$ is the function of oxygen atoms supplied and demanded. $N(O)_{supplied}$, $N(O)_{demanded}$ represent the number of equivalent oxygen atoms supplied and demanded in the supply-demand relationship, respectively. N_O represents the initial number of oxygen atoms.

First, we equate all initial oxygen atoms as bridge oxygen atoms, and two polyhedrons share a bridge oxygen atom. Therefore, the equivalent oxygen atoms that the system can supply are the product of

twice the initial oxygen atoms and the limit factor. It should be emphasized that the initial oxygen atom is the number of oxygen atoms when the system is set. Then, it is hardly possible for all oxygen atoms in the system to be equivalent to bridge oxygen atoms, so the limit factor R is used for correction. R represents the limit factor, that is, the maximum ratio of all oxygen atoms equivalent to BO. The calculation idea of R is that all types of oxygen atoms in all sample is supposed to be BO, and then take the percentage of all samples average value. The NBO is equivalent to 0.5 BO, and the TO is equivalent to 1.5 bridging oxygen. Data statistics of NBO, BO and TO are performed for all samples, and the equivalent calculation in equation (4) is performed. N_{sample} represents the sample size. The larger the sample size, the closer the limit factor is to reality. P_{NBO}, P_{BO} and P_{TO} respectively represents the percentage content of NBO, BO and oxygen triclusters (TO) in the sample. Finally, the calculation idea of $N(O)_{demanded}$ is to count the total number of oxygen atoms required by polyhedrons with different coordination numbers. N_i is the total number of cations corresponding to different coordination structures. P is the percentage content, and the i is the coordination number of polyhedrons.

After analyzing the atomic structure, the content of different types of oxygen atoms can be obtained as shown in Table S3.

Table S3. The content of different types of oxygen atoms

Basicity	Samples	FO	NBO	BO	TO
B=0.5	B1T1	0.085	15.789	66.187	15.381
	B1T2	0.061	11.958	65.831	18.632
	B1T3	0.052	8.974	62.222	23.258
	B1T4	0.031	6.229	60.152	27.398
	B1T5	0.013	5.652	58.326	29.231
	B1T6	0.005	4.265	57.265	31.231
B=0.9	B2T1	0.272	35.661	54.241	8.824
	B2T2	0.19	28.723	58.503	11.131
	B2T3	0.108	22.553	60.164	14.194

	B2T4	0.072	17.212	59.434	18.711
	B2T5	0.068	12.616	57.894	22.232
	B2T6	0.027	10.525	56.072	28.041
B=1.3	B3T1	0.63	45.382	45.767	7.424
	B3T2	0.63	45.382	45.767	7.424
	B3T3	0.606	37.494	50.179	10.362
	B3T4	0.448	29.476	53.918	13.027
	B3T5	0.281	23.636	56.877	16.296
	B3T6	0.196	18.083	56.01	20.24
B=1.7	B4T1	4.321	46.949	39.46	7.364
	B4T2	2.43	44.884	44.199	7.671
	B4T3	1.984	38.198	48.277	11.131
	B4T4	1.691	30.127	53.012	13.91
	B4T5	1.314	24.323	54.426	17.416
	B4T6	1.261	17.885	55.114	21.526

After the calculation of Equation 3, there is the result that R=0.92-0.93.

The calculation results of $N(O)_{supplied}$ and $N(O)_{demanded}$ are shown in Table S4.

Table S4. The calculation results of $N(O)_{supplied}$ and $N(O)_{demanded}$

$N(O)_{supplied}$	$N(O)_{demanded}$	$\Delta(O)$
11653	12152	-499
11690	12809	-1119
11724	13459	-1735
11759	14114	-2355
11800	14766	-2966
11839	15425	-3586
11294	10168	1126
11350	10830	520
11404	11486	-82
11459	12100	-641
11515	12764	-1249
11573	13864	-2291
11043	9111	1932
11112	9900	1212
11182	10645	537
11251	11279	-28
11322	12051	-729

11393	12792	-1399
10855	8305	2550
10937	8730	2207
11019	9144	1875
11100	10531	569
11182	10850	332
11262	11060	202

The calculation results of this simulation listed in Table S5.

Table S5. Results of model calculation

Δ(Sample 1-6)	-499	-1119	-1735	-2355	-2966	-3586
Δ(Sample 7-12)	1126	519	-82	-640	-1249	-2291
Δ(Sample 13-18)	1932	1212	538	-28	-730	-1400
Δ(Sample 19-24)	2550	2207	1874	569	332	202

2.4. Applicability Verification of Supply-Demand Model

In order to verify the universality of the supply-demand relationship model and theory, we performed the above calculations on the existing publication [14, 15] on the amphoteric behavior of oxides. The result is shown in Figure S6.

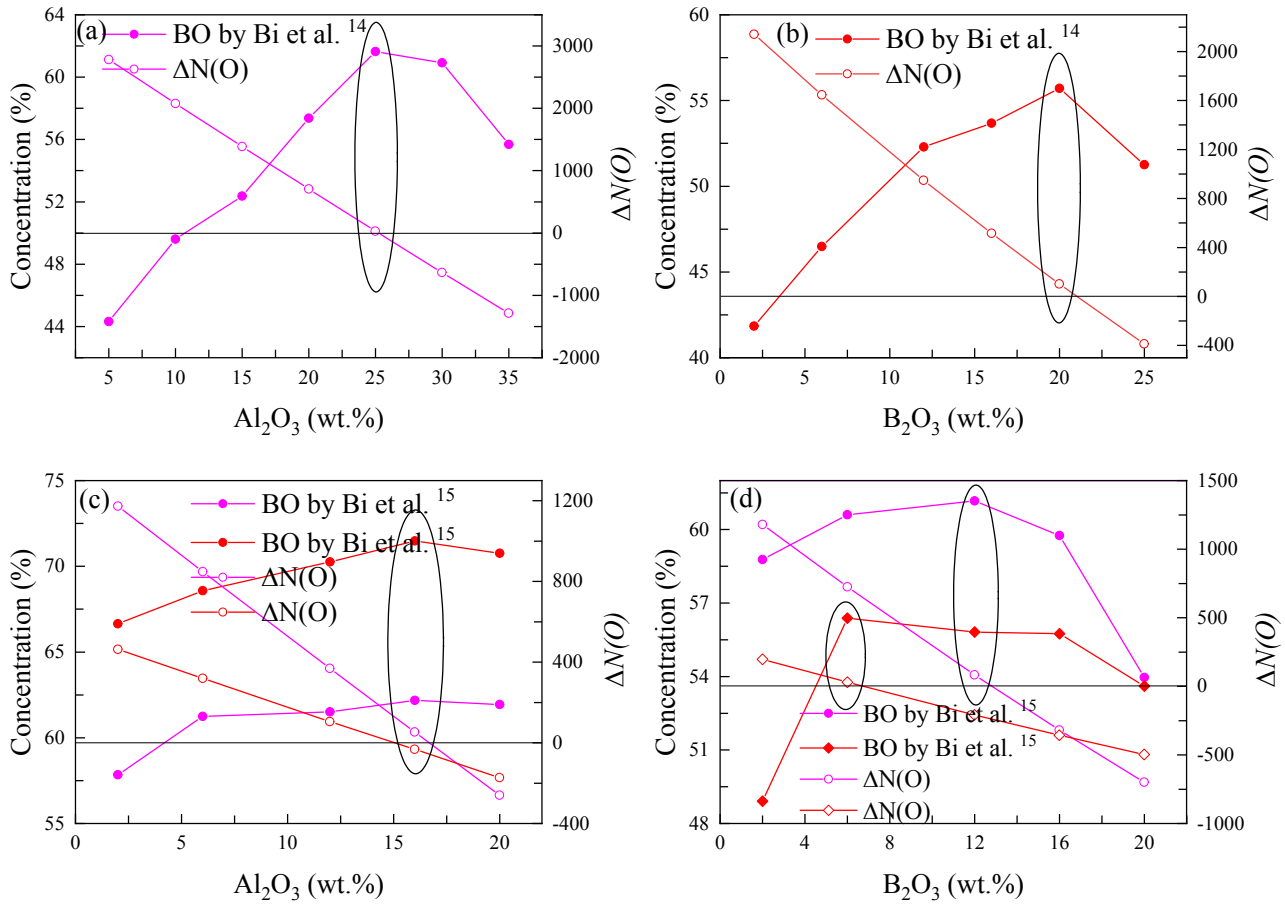

Figure S6. The calculation results of the supply-demand relationship model on the existing publications: (a-b) the data of bridge oxygen comes from the research results of SiO_2-CaO-Al_2O_3 and SiO_2-CaO-B_2O_3 systems by Bi et al. [14]; (c-d) the data of bridge oxygen comes from the research results of SiO_2-CaO-Al_2O_3-B_2O_3 systems by Bi et al. [15]. (a-b) Reprinted (Adapted or Reprinted in part) with permission from [Bi, Z.; Li, K.; Jiang, C.; Zhang, J.; Ma, S. Effects of amphoteric oxide (Al_2O_3 and B_2O_3) on the structure and properties of SiO_2-CaO melts by molecular dynamics simulation. Journal of

Non-Crystalline Solids. 2021, 559, 120687.] Copyright [2021], with permission from [Journal of Non-Crystalline Solids]. (c-d) Reprinted (Adapted or Reprinted in part) with permission from [Bi, Z.; Li, K.; Jiang, C.; Zhang, J.; Ma, S.; Sun, M.; Wang, Z.; Li, H. Performance and transition mechanism from acidity to basicity of amphoteric oxides (Al_2O_3 and B_2O_3) in SiO_2–CaO–Al_2O_3–B_2O_3 system: A molecular dynamics study. Ceramics International. 2021, 47, 12252-12260.] Copyright [2021], with permission from [Ceramics International].

The calculation results of the supply-demand relationship model of oxides in Figure S6 show that the difference curves of the supply-demand relationship of the systems SiO_2-CaO-Al_2O_3, SiO_2-CaO-B_2O_3 and SiO_2-CaO-Al_2O_3-B_2O_3 do possess the clear zero points, and the zero points are indeed near the concentration points of the amphoteric transition.

For more calculation details, see Table S6-S9

Table S6. The esults of the supply-demand relationship model of SiO_2-CaO-Al_2O_3 system [14]. Reprinted (Adapted or Reprinted in part) with permission from [Bi, Z.; Li, K.; Jiang, C.; Zhang, J.; Ma, S. Effects of amphoteric oxide (Al2O3 and B2O3) on the structure and properties of SiO2-CaO melts by molecular dynamics simulation. Journal of Non-Crystalline Solids. 2021, 559, 120687.] Copyright [2021], with permission from [Journal of Non-Crystalline Solids]

Si	Ca	Al	O	$N(O)_{supplied}$	$N(O)_{demanded}$	$\Delta(O)$
1746	2095	230	5932	10914.88	8134	2780.88
1641	1969	456	5935	10920.4	8844	2076.4
1538	1846	678	5939	10927.76	9542	1385.76
1436	1724	896	5940	10929.6	10224	705.6
1336	1604	1114	5947	10942.48	10914	28.48
1317	1580	1156	5948	10944.32	11048	-103.68
1297	1556	1198	5947	10942.48	11178	-235.52

1277	1533	1242	5950	10948	11318	-370
1258	1509	1284	5951	10949.84	11452	-502.16
1238	1486	1326	5951	10949.84	11582	-632.16
1141	1369	1536	5955	10957.2	12244	-1286.8

Table S7. The esults of the supply-demand relationship model of SiO_2-CaO-B_2O_3 system [14]. Reprinted (Adapted or Reprinted in part) with permission from [Bi, Z.; Li, K.; Jiang, C.; Zhang, J.; Ma, S. Effects of amphoteric oxide (Al2O3 and B2O3) on the structure and properties of SiO2-CaO melts by molecular dynamics simulation. Journal of Non-Crystalline Solids. 2021, 559, 120687.] Copyright [2021], with permission from [Journal of Non-Crystalline Solids]

Si	Ca	B	O	$N(O)_{supplied}$	$N(O)_{demanded}$	$\Delta(O)$
1790	2148	134	5929	10553.62	8412	2141.62
1671	2005	390	5932	10558.96	8912.4	1646.56
1504	1805	752	5941	10574.98	9625.6	949.38
1400	1680	976	5944	10580.32	10064	516.32
1301	1561	1190	5948	10587.44	10484.4	103.04
1277	1532	1242	5949	10589.22	10586.8	2.42
1253	1504	1294	5951	10592.78	10689.2	-96.42
1230	1476	1344	5952	10594.56	10788	-193.44
1206	1448	1394	5951	10592.78	10882.4	-289.62
1184	1420	1444	5954	10598.12	10985.6	-387.48

Table S8. The results of the supply-demand relationship model of SiO_2-CaO-Al_2O_3-B_2O_3 system [15]. Reprinted (Adapted or Reprinted in part) with permission from [Bi, Z.; Li, K.; Jiang, C.; Zhang, J.; Ma, S.; Sun, M.; Wang, Z.; Li, H. Performance and transition mechanism from acidity to basicity of amphoteric oxides (Al2O3 and B2O3) in SiO2–CaO–Al2O3–B2O3 system: A molecular dynamics study. Ceramics International. 2021, 47, 12252-12260.] Copyright [2021], with permission from [Ceramics International]

Si	Ca	Al	B	O	$N(O)_{supplied}$	$N(O)_{demanded}$	$\Delta(O)$

1686	2023	226	132	5932	10558.96	8402	2156.96
1570	1885	220	388	5937	10567.86	8932	1635.86
1409	1690	212	746	5945	10582.1	9680	902.1
1307	1569	208	970	5950	10591	10148	443
1211	1454	202	1182	5952	10594.56	10582	12.56
1382	1658	884	130	5943	11648.28	10468	1180.28
1277	1533	862	378	5947	11656.12	10930	726.12
1130	1356	830	730	5956	11673.76	11590	83.76
1037	1245	810	950	5959	11679.64	11998	-318.36
950	1139	790	1158	5961	11683.56	12382	-698.44
1092	1310	1514	128	5957	11914	11716.4	197.6
996	1196	1476	372	5960	11920	11889.6	30.4
862	1035	1424	714	5966	11932	12140.4	-208.4
778	934	1390	930	5970	11940	12296	-356
698	838	1358	1134	5972	11944	12440.8	-496.8

Table S9. The results of the supply-demand relationship model of SiO_2-CaO-Al_2O_3-B_2O_3 system [15]. Reprinted (Adapted or Reprinted in part) with permission from [Bi, Z.; Li, K.; Jiang, C.; Zhang, J.; Ma, S.; Sun, M.; Wang, Z.; Li, H. Performance and transition mechanism from acidity to basicity of amphoteric oxides (Al2O3 and B2O3) in SiO2–CaO–Al2O3–B2O3 system: A molecular dynamics study. Ceramics International. 2021, 47, 12252-12260.] Copyright [2021], with permission from [Ceramics International]

Si	Ca	Al	B	O	$N(O)_{supplied}$	$N(O)_{demanded}$	$\Delta(O)$
1659	1991	326	90	5933	10560.74	8210	2350.74
1579	1894	324	266	5937	10567.86	8410	2157.86
1459	1751	322	526	5941	10574.98	8702	1872.98
1380	1657	320	698	5944	10580.32	8894	1686.32
1303	1563	318	868	5948	10587.44	9088	1499.44
1265	1518	1186	82	5950	11543	10369.2	1173.8
1193	1432	1180	242	5951	11544.94	10696	848.94
1088	1305	1170	480	5956	11554.64	11186	368.64
1018	1222	1164	636	5958	11558.52	11504.8	53.72
950	1139	1158	790	5961	11564.34	11823.6	-259.26
936	1124	1904	74	5963	12045.26	11582	463.26

872	1047	1894	222	5965	12049.3	11730	319.3
778	933	1880	440	5969	12057.38	11952	105.38
716	859	1870	584	5972	12063.44	12096	-32.56
654	785	1862	726	5975	12069.5	12242	-172.5

In addition, the research of Chen et al.[16] is calculated by the model of supply and demand, and the results show that the model of supply and demand is also applicable to Chen et al.[16] Firstly, the number of oxygen atoms supplied by the system is determined by the system setting in this paper. Then, the amount of oxygen demanded by the system and the limit factor can be calculated by the coordination numbers of Si and Al and the corresponding coordination numbers. Finally, the supply and demand function is calculated to judge the relationship between the zero point and the turning point of Al2O3.

Figure S7 is the data figure of atomic structure change in molecular dynamics study by Chen et al. Through data capture, the contents of various oxygen and coordination of Al in this study are counted in Table S10. Table S11 counts the number of oxygen atoms required by the system and the size of the limit factor. The related data of Table S10 and Table S11 are plotted as Figure S8. By analyzing the turning point of the bridge oxygen curve and the zero point of the supply-demand function in Figure S8, it can be seen that the calculation model of supply-demand relationship is also applicable to Dr. Chen's research on the amphoteric behavior of oxides. The following analysis authors have been added to the Supporting Information.

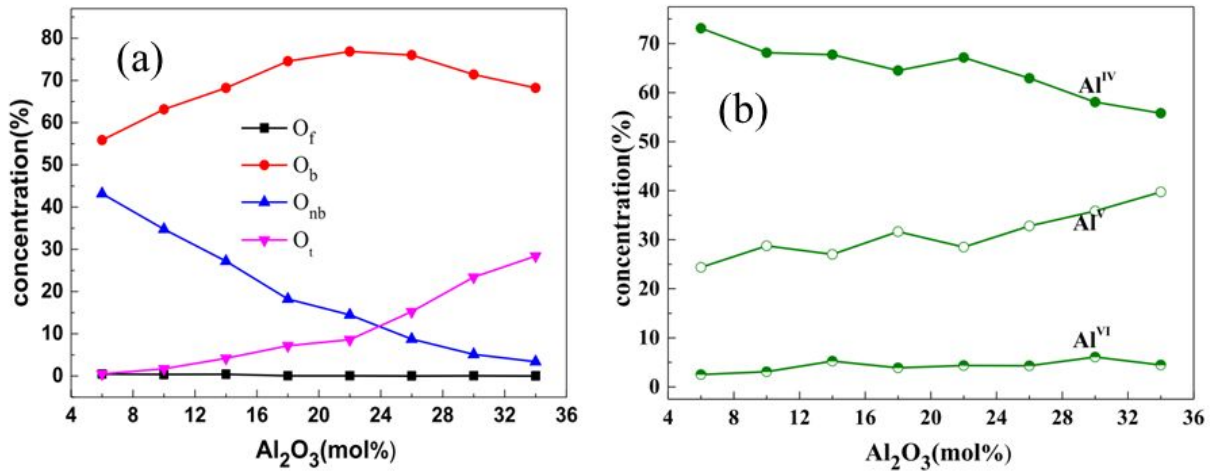

Figure S7 Changes of oxygen network structure and coordination number of Al in Dr. Chen's research[16]. Reprinted (Adapted or Reprinted in part) with permission from [Chen, Y.; Pan, W.; Jia, B.; Wang, Q.; Zhang, X.; Wang, Q.; He, S. Effects of the amphoteric behavior of Al2O3 on the structure and properties of CaO-SiO2-Al2O3 melts by molecular dynamics. Journal of Non-Crystalline Solids. 2021, 552, 120435.] Copyright [2021], with permission from [Journal of Non-Crystalline Solids].

Table S10 The contents of various oxygen and coordination of Al. Reprinted (Adapted or Reprinted in part) with permission from [Chen, Y.; Pan, W.; Jia, B.; Wang, Q.; Zhang, X.; Wang, Q.; He, S. Effects of the amphoteric behavior of Al2O3 on the structure and properties of CaO-SiO2-Al2O3 melts by molecular dynamics. Journal of Non-Crystalline Solids. 2021, 552, 120435.] Copyright [2021], with permission from [Journal of Non-Crystalline Solids]

Al2O3 (mol.%)	NBO	BO	TO	4-coordination	5-coordination	6-coordination
6.00	43.11	55.89	0.37	73.44	24.39	2.17
10.00	34.70	63.20	1.46	68.28	28.69	3.03
14.00	27.03	67.95	4.38	67.70	27.25	5.04
18.00	18.26	74.52	6.94	64.26	31.84	3.89
22.00	14.61	76.71	8.77	67.42	28.40	4.18
26.00	8.77	75.62	14.98	63.40	32.70	3.89
30.00	5.11	71.23	23.38	57.95	36.15	5.90
34.00	3.29	68.68	28.13	55.94	39.30	4.75

Table S11 Calculation results of supply-demand model

	Al2O3	supplied	demanded	ΔN
R=0.95	6.00	4560	3616.288	943.7123
	10.00	4560	3880.787	679.2131
	14.00	4560	4130.357	429.6426
	18.00	4560	4369.4	190.6
	22.00	4560	4568.486	-8.48607
	26.00	4560	4787.246	-227.246
	30.00	4560	5029.877	-469.877
	34.00	4560	5220.349	-660.349

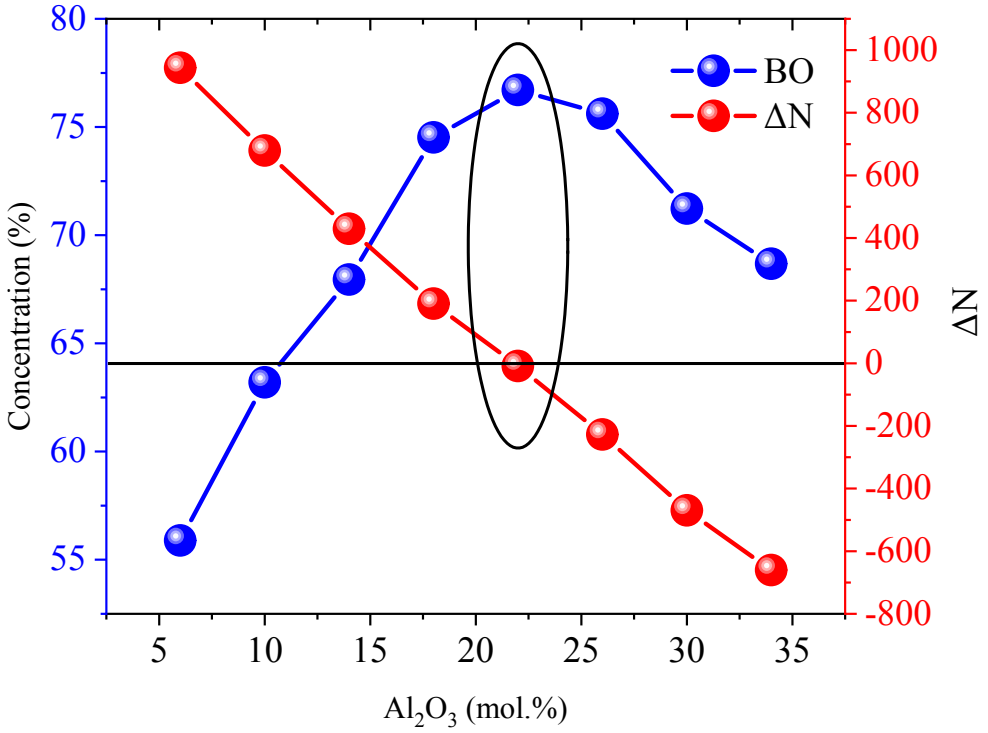

Figure S8 Calculation results of supply-demand model[16]. Reprinted (Adapted or Reprinted in part) with permission from [Chen, Y.; Pan, W.; Jia, B.; Wang, Q.; Zhang, X.; Wang, Q.; He, S. Effects of the amphoteric behavior of Al2O3 on the structure and properties of CaO-SiO2-Al2O3 melts by molecular dynamics. Journal of Non-Crystalline Solids. 2021, 552, 120435.] Copyright [2021], with permission from [Journal of Non-Crystalline Solids].

References

(1) Zhang, S.; Zhang, X.; Bai, C.; Wen, L.; Lv, X. Effect of TiO_2 content on the structure of CaO-SiO_2-TiO_2 system by molecular dynamics simulation. *ISIJ Int.* 2013, *53*, 1131-1137.

(2) Yao, T.; He, S.; Wu, T.; Wang, Q. Molecular dynamics simulations of microstructural properties of CaO-SiO_2-TiO_2 fluorine-free slag systems. *Ironmak. Steelmak.* 2017, *44*, 551-558.

(3) Zhao, G.; Perilla, J. R.; Yufenyuy, E. L.; Meng, X.; Chen, B.; Ning, J.; Ahn, J.; Gronenborn, A. M.; Schulten, K.; Aiken, C., et al. Mature HIV-1 capsid structure by cryo-electron microscopy and all-atom molecular dynamics. *Nature* 2013, *497*, 643-6.

(4) Roux, S. L.; Petkov, V. ISAACS-interactive structure analysis of amorphous and crystalline systems. *Journal of Applied Crystallography* 2010, *43*, 181-185.

(5) Loken, C.; Gruner, D.; Groer, L.; Peltier, R.; Bunn, N.; Craig, M.; Henriques, T.; Dempsey, J.; Yu, C.; Chen, J., et al. SciNet: Lessons Learned from Building a Power-efficient Top-20 System and Data Centre. *Journal of Physics: Conference Series* 2010, *256*.

(6) Ponce, M.; van Zon, R.; Northrup, S.; Gruner, D.; Chen, J.; Ertinaz, F.; Fedoseev, A.; Groer, L.; Mao, F.; Mundim, B. C., et al. Deploying a Top-100 Supercomputer for Large Parallel Workloads: the Niagara Supercomputer. 2019, 1-8.

(7) Sahoo, M.; Yadav, A.; Jha, S.; Bhattacharyya, D.; Mathews, T.; Sahoo, N.; Dash, S.; Tyagi, A. Nitrogen location and Ti-O bond distances in pristine and N-doped TiO_2 anatase thin films by X-ray absorption studies. *The Journal of Physical Chemistry C* 2015, *119*, 17640-17647.

(8) Li, K.; Zhang, J.; Bouhadja, M.; Barati, M.; Yang, T.; Liu, Z.; Sahajwall, V.; Singh, C. V.; Su, B.; Khanna, R. A molecular dynamic simulation on the factors influencing the fluidity of molten coke ash during alkalization with K_2O and Na_2O. *Chem. Eng. J.* 2017, *313*, 1184-1193.

(9) Jiang, N.; Su, D.; Spence, J. Determination of Ti coordination from pre-edge peaks in Ti K-edge XANES. *Physical Review B* 2007, *76*, 214117.

(10) Plimpton, S. Fast parallel algorithms for short-range molecular dynamics. *J. Comput. Phys.* 1995, *117*, 1-19.

(11) Haffad, D.; Chambellan, A.; Lavalley, J. Propan-2-ol transformation on simple metal oxides TiO_2, ZrO_2 and CeO_2. *Journal of Molecular Catalysis A: Chemical* 2001, *168*, 153-164.

(12) Bakbolat, B.; Daulbayev, C.; Sultanov, F.; Beissenov, R.; Umirzakov, A.; Mereke, A.; Bekbaev, A.; Chuprakov, I. Recent Developments of TiO_2-Based Photocatalysis in the Hydrogen Evolution and Photodegradation: A Review. *Nanomaterials* 2020, *10*, 1790.

(13) Li, Z.; Qi, M.; Tu, C.; Wang, W.; Chen, J.; Wang, A. Highly efficient removal of chlorotetracycline from aqueous solution using graphene oxide/TiO_2 composite: Properties and mechanism. *Applied Surface Science* 2017, *425*, 765-775.

(14) Bi, Z.; Li, K.; Jiang, C.; Zhang, J.; Ma, S. Effects of amphoteric oxide (Al_2O_3 and B_2O_3) on the structure and properties of SiO_2-CaO melts by molecular dynamics simulation. *J Non Cryst Solids* 2021, *559*, 120687.

(15) Bi, Z.; Li, K.; Jiang, C.; Zhang, J.; Ma, S.; Sun, M.; Wang, Z.; Li, H. Performance and transition mechanism from acidity to basicity of amphoteric oxides (Al_2O_3 and B_2O_3) in SiO_2-CaO-Al_2O_3-B_2O_3 system: A molecular dynamics study. *Ceram. Int.* 2021, *47*, 12252-12260.

(16) Chen, Y.; Pan, W.; Jia, B.; Wang, Q.; Zhang, X.; Wang, Q.; He, S. Effects of the

amphoteric behavior of Al_2O_3 on the structure and properties of CaO-SiO_2-Al_2O_3 melts by molecular dynamics. *J Non Cryst Solids* 2021, *552*, 120435.